ELSEVIER

Journal of Crystal Growth 237–239 (2002) 2035–2040

JOURNAL OF CRYSTAL GROWTH

www.elsevier.com/locate/jcrysgro

Self-organized growth of nanosized flat dots and vertical magnetic Co pillars on Au(1 1 1)

O. Fruchart[a,b,*], G. Renaud[c], J.-P. Deville[d], A. Barbier[c], F. Scheurer[d], M. Klaua[b], J. Barthel[b], M. Noblet[c], O. Ulrich[c], J. Mané-Mané[d], J. Kirschner[b]

[a] *Laboratoire Louis Néel, CNRS, BP166, F-38042, Grenoble Cedex 9, France*
[b] *MPI für Mikrostrukturphysik, Weinberg 2, D-06120 Halle, Germany*
[c] *DRFMC/SP2M/IRS (CEA), 17 Rue des Martyrs, F-38054 Grenoble Cedex 9, France*
[d] *IPCMS (UMR 7504 CNRS-ULP), 23 rue du Loess, F-67037 Strasbourg Cedex, France*

Abstract

We report various experiments that cast some light on the growth process of self-organized dots and vertical Co pillars on Au(1 1 1). We first report grazing incidence small angle X-ray scattering (GISAXS) on Co dots and films, that allowed us to perform a crystallographic study of the order in the self-organized array, and also yielded a statistical view of the coalescence process. We then report scanning tunneling microscopy (STM) and spectroscopy (STS) images performed during the course of vertical growth. Details about the atomic growth process and the possible influence of the growth technique used are reported.

PACS: 68.65.+g; 68.35.Bs; 61.16.Ch; 61.10.Eq

Keywords: A1. Grazing incidence small angle X-ray diffusion; A1. Low dimensional structures; A1. Nanostructures; A1. Surface processes; A3. Molecular beam epitaxy; B2. Magnetic materials

1. Introduction

Self-organized (SO) epitaxial growth has received much attention for its ability to produce spontaneously high quality nanostructures down to the low nanometer range. Whereas epitaxial SO was first demonstrated to yield rather flat structures in the first stages of growth, a new search path consists in growing three-dimensional (3D) self-organized structures by sequential deposition [1,2]. Among the motivations are pushing the limits of SO versatility, as well as potential applications that usually require larger amounts of active material than simply fractions of atomic layers.

Whereas 3D SO usually consists of dot stackings, it was shown recently that continuous vertical structures may be grown as well. This way, laterally ordered arrays of vertical magnetic Co pillars with a density of more than $10^{12}\,cm^{-2}$ [2] were fabricated. The purpose of this article is to report experiments casting some light on effects relevant to vertical growth. We first report grazing incidence small angle X-ray scattering (GISAXS) experiments performed on mono-atomic deposits,

*Corresponding author. Laboratoire Louis Néel, CNRS, BP166, F-38042, Grenoble Cedex 9, France. Tel.: +33476-887920; fax: +33476-881191.

E-mail address: fruch@polycnrs-gre.fr (O. Fruchart).

0022-0248/02/$ - see front matter
PII: S0022-0248(01)02305-3

from flat Co dots to continuous Co films. We then report scanning tunneling microscopy (STM) and scanning tunneling spectroscopy (STS) experiments carried out on flat dots and during the course of vertical growth by sequential Co/Au deposition.

2. Flat dots and films investigated by GISAXS

In GISAXS an X-ray beam is shone at grazing incidence on a sample and a surface-sensitive two-dimensional (2D) diffusion pattern is collected, that reflects correlations at the 1–100 nm nanometer scale [3]. In the case of self-organized surfaces this yields information on the reciprocal space of the superstructure. As in techniques with a similar geometry like reflection high energy electron diffraction, the 2D pattern results from the tangent intercept of the low-curvature Ewald Sphere with the superstructure reciprocal space truncation rods perpendicular to the sample surface, which yield streaks patterns.

Our GISAXS experiments were performed in situ on a fully dedicated experimental setup built on the ID32 beamline at ESRF. No window is placed before the sample and the beam is defined by two successive pairs of motorized slits, thus minimizing background scattering. Diffusion patterns were collected on a 16-bit X-ray CCD detector placed just after a beryllium window. A motorized Ta beam-stop was introduced between the exit Be window and the 2D detector. The combination of high flux, grazing incidence, on-surface structures, low background and before-growth background subtraction are mandatory to achieve a high signal-to-noise ratio well below one atomic layer.

The SO Co dot arrays on Au(1 1 1) are made of parallel rows of dots (see Fig. 1a) and have a rectangular mean unit cell. Streaks arising from truncation rods of this periodic array are already clearly visible at 0.1 AL (see Fig. 1b and c). The streaks with beam azimuth along [1 $\bar{1}$ 0] are very narrow, which shows that the degree of order along the lines is of crystallographic quality. This was expected as the period Λ along the lines is directly related to the $N \times \sqrt{3}$ Au reconstruction

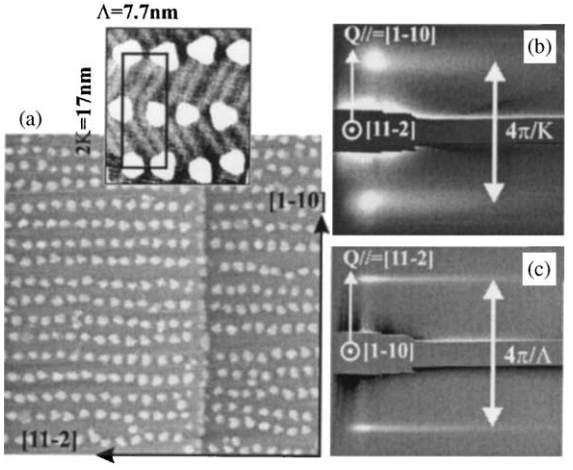

Fig. 1. (a) 150×150 nm STM image of flat Co dots on Au(1 1 1). The mean super-cell is shown in inset. GISAXS patterns with X-ray beam along (b) [1 1 $\bar{2}$] and (c) [1 $\bar{1}$ 0]. The sample surface is vertical and located on the left hand side of the patterns.

[4], with $N \simeq 22-23$. The streaks with beam azimuth along [1 1 $\bar{2}$] are much broader, which reveals a broad distribution of inter-line nearest neighbors distance κ, resulting in a liquid-type order perpendicular to the lines. This can be understood as κ is related to the so-called herring-bone superstructure that results from a more subtle energy balance than the basic $N \times \sqrt{3}$ structure, and is therefore more liable to fluctuate. In the experiment reported here we found $\lambda = 7.7$ nm, and $\kappa = 8.5$ nm with standard deviation $\Delta\kappa = 2.05$ nm. Besides, three types of domains of Co arrays were found, each rotated with respect to each other by $\pm 120^\circ$, as already known and in accordance with the three-fold symmetry of a Au(1 1 1) crystal. This allows us to draw a sketch of the reciprocal space of the Co/Au(1 1 1) supercrystalline array (see Fig. 2).

We monitored GISAXS patterns for Co thickness t ranging from 0.1 to 15 AL. In this paper we restrict the analysis to the intensity $I_1(t)$ of the first and $I_2(t)$ of the second order narrow [1 1 $\bar{2}$] peaks probing intra-line order, measured at their maximum along the direction perpendicular to the surface, and integrated along $Q_\parallel$ (see Fig. 3). In a first crude approach we calculate $I_1(t)$ and $I_2(t)$ from one single line of disk-shaped dots with

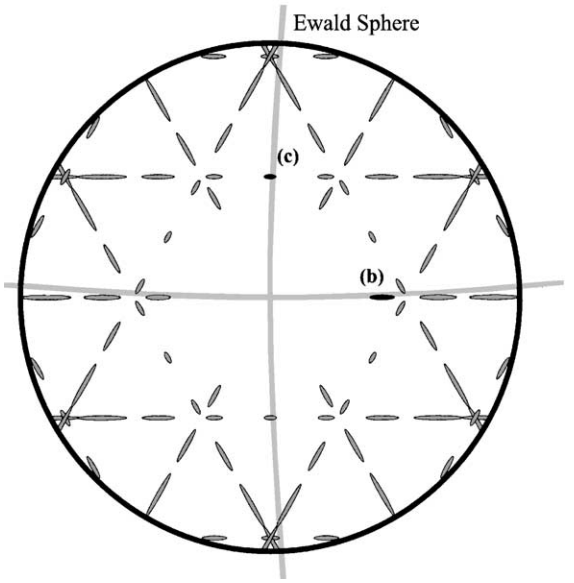

Fig. 2. Sketch of the truncation rods section of the Co dot array super-reciprocal-space accessible to CCD camera. The Ewald sphere and the spots reported in Fig. 1b and c are labeled.

diameter d. The reciprocal space of a line of dots for a diffusion vector parallel to the line is the product of Dirac functions associated with the real-space period Λ, with the shape factor of a disk-shaped dot involving the first order Bessel function J_1. The predicted variation of $I_1(t)$ and $I_2(t)/I_1(t)$ is displayed in Fig. 3.

We first discuss I_2/I_1. The predicted cancellation of I_2/I_1 results from the superposition of the second order Dirac peak with the first zero of J_1. This should occur for $d \simeq 0.61\Lambda$. Experimentally I_2/I_1 reaches nearly perfect cancellation before increasing again tenfold. This demonstrates the low dispersion of dots size and period. Most importantly, the knowledge of Λ and κ deduced above from streaks positions, added to the predicted cancellation of I_2/I_1, permits a precise thickness calibration and gives a firm ground to the discussion of I_1 found in the next paragraph. A more quantitative analysis of the experimental I_2/I_1 function will be reported elsewhere.

We finally discuss the behavior of $I_1(t)$. Within our crude model $I_1(t)$ should reach its maximum around 1.7 Å, then decrease rapidly and cancel

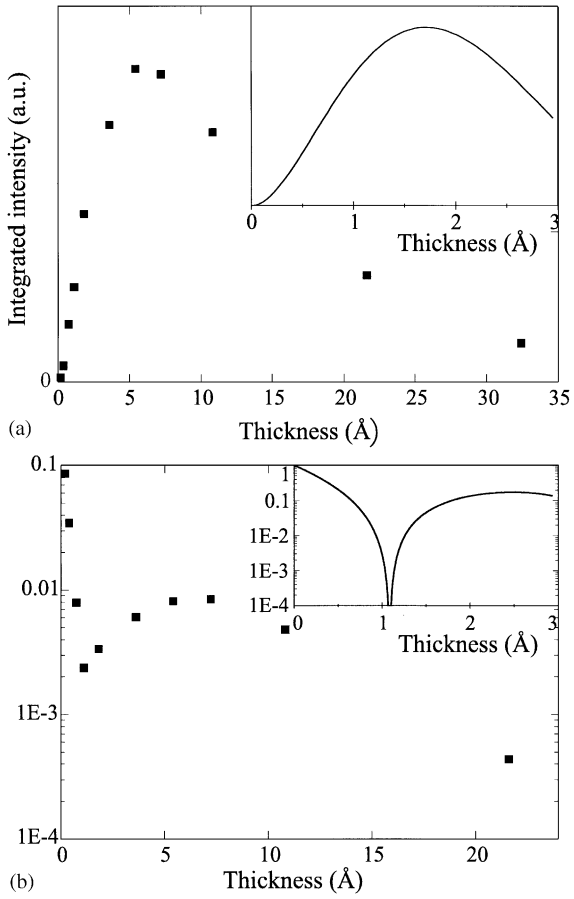

Fig. 3. Experimental intensity of [1 1 $\bar{2}$] Bragg streaks (solid squares), with predictions for a single line of disk-shaped dots shown in inset: (a) first order, (b) ratio of second over first order.

when all dots coalesce into a continuous film, around 2 AL. On the contrary experimental $I_1(t)$ increases up to 6 Å ($\sim$3 AL), then decreases extremely slowly. This reveals that even 'thick' Co films retain some kind of memory of the initial self-organized nucleation stage. To what extent and in what form this memory is stored is not clear to date. It was known from STM that surface roughness after 2 AL deposition is 1–2 AL high, with patterns resembling those of the initial array [5]. The GISAXS diffracted intensity expected from this roughness solely should not exceed that obtained around 1 AL. This suggests that some of the diffracted intensity must come from the

microstructure due to imperfect coalescence of the buried Co layers, and that real coalescence does not occur before 5–10 AL are deposited. The form taken by the microstructure, i.e. grooves, Au atoms coming from the substrate, or both, is not clear yet.

In conclusion to this section, preliminary analysis of GISAXS experiments performed in situ on self-organized Co/Au(1 1 1) suggests that coalescence of the dots into a film is a progressive process not fully complete even after deposition of 15 AL of Co. This, combined with the immiscibility of Co and Au, is a clue to explain why sequential deposition of Co and Au so easily preserves the initial self-organized pattern, as reported below.

3. Growth of vertical pillars by sequential deposition

We very briefly remind the reader of the principle of self-organized growth of vertical Co pillars in Au(1 1 1). The starting point is deposition at 300 K on Au(1 1 1) of a nominal thickness of $(2x)$ AL of Co (typically $0.10 < x < 0.35$), yielding a conventional array of flat Co dots, mostly 2 AL-high [6]. This array is then covered at 475 K by $(3 - 2x)$AL Au, yielding a smooth surface. Further deposition consists in proceeding many times to the following two steps at a constant temperature of 525 K. Step 1: x AL deposited Co nucleate as dots in direct contact with the existing buried Co dots, by an atomic exchange process with Au, thus heightening the Co dots by 1 AL. Step 2: $(1 - x)$ AL Au are deposited to heighten the matrix by 1 AL as well. More details can be found in Refs. [2,7].

Earlier proofs of Co/Au(1 1 1) vertical growth were based on two indirect facts: height analysis of topographic STM images, and magnetic evaluation of the pillars volume [2,7]. Fig. 4 shows topographic and spectroscopic images during the course of vertical growth, after deposition of Co(0.1 AL) on Au(2.8 AL)/Co(0.2 AL)/Au. As the buried dots are initially covered by 1 AL Au, the fact that Co atoms are found solely and above all existing buried dots, demonstrates directly the occurrence of the Au/Co atomic exchange process. Fig. 4 also shows that the capping of some of the 3 AL-high dots is made of Co as well, whereas topographic analysis reveals a height of 2.3 Å, and thus could have induced us to think of a Au capping. The identification of Co capping confirms that Au atoms are hindered from covering existing Co dots, as suggested earlier from topographic STM images of interaction of steps with buried dots [7]. This latter effect is further confirmed by an observation on flat conventional dots. It was indeed known that for Co coverage above 0.5 AL some of the dots displayed height of 3 AL, although nothing was known about the capping composition, either Co or Au [8,9]. The topographic and spectroscopic images in Fig. 5 demonstrates that the capping is made of Co.

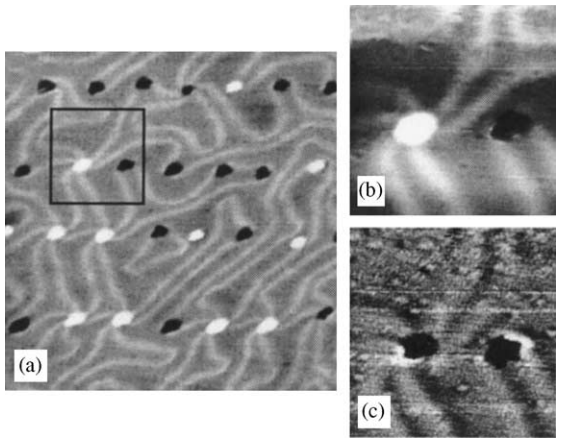

Fig. 4. (a) 50×50 nm STM image ($V = -1$ V; $I = -0.55$ nA) of sample Co(0.1 AL)/Au(2.8 AL)/Co(0.2 AL)/Au(1 1 1). The 15×15 nm square area is enlarged in (b) for topography and in (c) for $I(V)$ spectroscopy (I map recorded at $V = +1$ V, starting from $V = -0.94$ V and $I = -0.98$ nA feedback).

From the effects mentioned above it is clear that Au and Co are strongly induced to grow separately on the surface, so that the occurrence of vertical growth is not surprising. However these are only facts, that do not reveal the ground for such effects to happen. Fig. 6 shows flat Co dots of coverage $2x = 0.65$ AL, covered at 475 K by 2.5 AL Au. On most of the image 3 AL Au cover the initial Au surface, whereas the central and left islands holds 4 AL. The location of the buried 2 AL high Co dots can be traced thanks to the

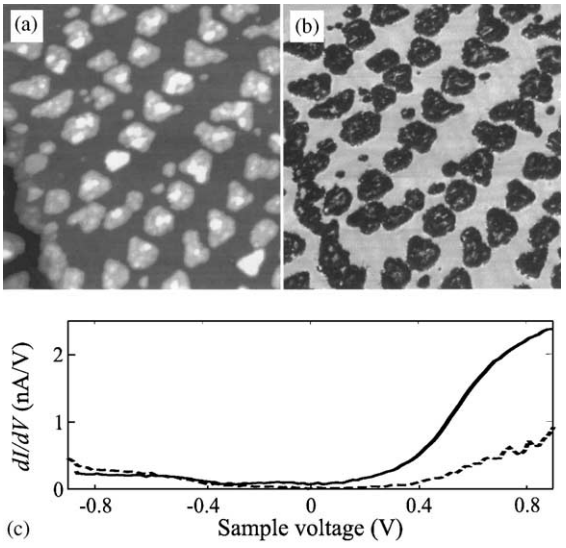

Fig. 5. 60×60 nm STM images of flat Co dots with 0.65 AL coverage. Co aggregation along a Au mono-atomic step is also seen in the bottom-left corner. (a) Topographic mode at $V = -0.885$ V; $I = -0.28$ nA; (b) spectroscopic mode: I map at $V = +0.9$ V; (c) typical dI/dV curve above Au (solid line) and Co (dotted line).

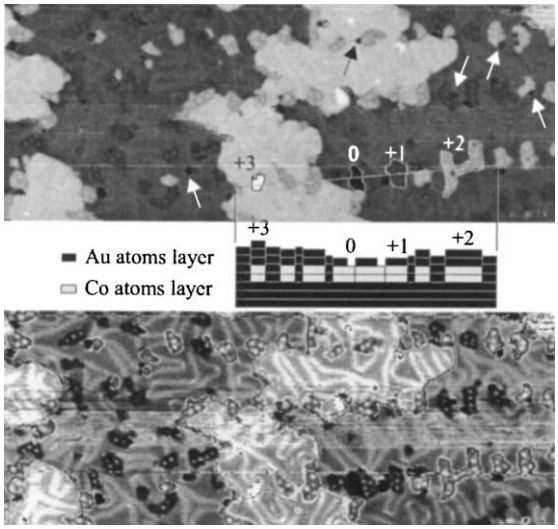

Fig. 6. 58×150 nm STM images of Au(2.5 AL)/Co(0.65 AL)/Au(1 1 1). Bottom: a multi-level gray scale was used to enhance the contrast on each atomic terrace level. A cross-sectional sketch is drawn.

height difference between Co and Au atoms [10,2]. On this image Co dots covered by 0, 1, 2 and 3 AL Au are highlighted, and a cross-sectional sketch is drawn. On the Au capping regularly spaced spots of height 0.4–0.6 Å are imaged, that from the 2 nm period are ascribed to dislocations of Au on Co. This confirms that the Co lattice parameter is nearly fully relaxed to its bulk value [11], and that even 1 AL of Au cannot cover Co without making dislocations. This certainly considerably diminishes the wetting energy of Co by Au, and may even make it unfavorable from a thermodynamic point of view. Besides, the occurrence of dislocations may favor atomic exchange processes, the same way conventional Co dots nucleate on the kinks of the Au herring-bone reconstruction after atomic exchange processes between Co adatoms and Au atoms from the substrate [12].[1] Lattice parameter mismatch and immiscibility are therefore thought to be crucial ingredients for vertical growth.

We finally discuss the influence of the growth technique. The growth of Au has always been performed with the use of a crucible, with a deposition rate of 0.35 AL min^{-1}. In Refs. [2,7] and Figs. 1–4 Co deposition was performed with the use of a mini electron beam evaporator loaded with a small Co rod, with a typical deposition rate of 0.02 AL min^{-1}. In the present paper Figs. 5 and 6 were obtained with Co evaporated from a crucible, with a deposition rate of 0.3 AL min^{-1}. A close inspection of Fig. 6 reveals that the Au capping is incomplete above most of the dots (see arrows), in the form of one or more nanometer-sized holes. This feature was not observed with deposition of Co from a rod. This feature is amplified during the course of vertical growth. Fig. 7 shows the sample surface after sequential deposition of $(7x)$ AL Co and $[7(1-x)]$ AL Au, capped with $(1-x)$ AL Au. A small fraction of the dots appears as craters. Cross-sections analysis reveals that the craters can be several AL deep, which excludes an effect solely due to non-capping by the latest deposited Au layer. The number of affected pillars remains nearly constant, but further growth leads to deeper holes. This effect did not occur with deposition of Co from a electron beam heated rod (EB). Three facts could be blamed for the difference with crucible

[1] For Ni/Au(1 1 1) see Ref. [13].

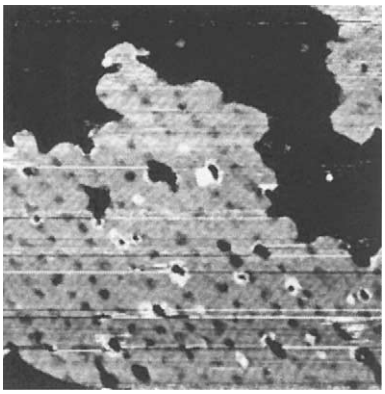

Fig. 7. 150×150 nm STM image after seven bilayers were deposited.

evaporation (CE). (1) The growth rate might be too high compared to that reached with EB to allow the atomic exchange process to occur above all pillars. (2) In EB a small fraction of the Co Beam is ionized and carries energetic species that may play a role in nucleation of the exchange process. (3) The vacuum during deposition was better for CE (10×10^{-11} mbar) than for EB (10×10^{-10} mbar), because in EB it is not possible to melt-outgas the rod before deposition. Gas adsorbates such as oxygen may play a surfactant role.

4. Conclusion

We have investigated effects that cast some light on the process of vertical self-organization of Co pillars on Au(1 1 1). GISAXS performed on flat Co dots and films reveals that coalescence into a uniform film is a very slow process not fully achieved at 15 AL, suggesting why Co/Au segregation and sequential deposition are favored. STM and STS performed during the course of vertical growth give for the first time a direct chemical proof of vertical growth. It is suggested that immiscibility and lattice parameter mismatch are crucial ingredients for vertical growth. Finally preliminary results suggest that parameters such as gas contamination and growth rate might play a role.

Acknowledgements

We are grateful to G. Kroder (MPI) for technical support.

References

[1] Q. Xie, A. Madhukar, P. Chen, N. Kobayashi, Phys. Rev. Lett. 75 (1995) 2542.
[2] O. Fruchart, M. Klaua, J. Barthel, J. Kirschner, Phys. Rev. Lett. 83 (1999) 2769.
[3] J.R. Levine, J. Cohen, Y. Chung, P. Georgopoulos, J. Appl. Cryst. 22 (1989) 528.
[4] J. Barth, H. Brune, G. Ertl, R. Behm, Phys. Rev. B 42 (1990) 9307.
[5] S. Padovani, I. Chado, F. Scheurer, J.-P. Bucher, Phys. Rev. B. 59 (1999) 11887.
[6] B. Voigtländer, G. Meyer, N.M. Amer, Phys. Rev. B 44 (1991) 10354.
[7] O. Fruchart, M. Klaua, J. Barthel, J. Kirschner, Appl. Surf. Sci. 162–163 (2000) 529, proceeding of ACSIN5.
[8] C. Tölkes, P. Zeppenfeld, M.A. Krzyzowski, R. David, G. Comsa, Phys. Rev. B 55 (1997) 13932.
[9] S. Padovani, F. Scheurer, J.-P. Bucher, Europhys. Lett. 45 (1999) 327.
[10] J. Wollschläger, N. Amer, Surf. Sci. 277 (1992) 1.
[11] N. Marsot, R. Belkhou, H. Magnan, P.L. Fèvre, C. Guillot, D. Chandesris, Phys. Rev. B 59 (1999) 3135.
[12] S. Rousset, private communication.
[13] J.A. Meyer, I.D. Baikie, E. Kopatzki, R.J. Behm, Surf. Sci. 365 (1996) L647.